Aerosol Science and Technology, 48:689–697, 2014

ISSN: 0278-6826 print / 1521-7388 online
DOI: 10.1080/02786826.2014.917758

Mixing State of Black Carbon Aerosol in a Heavily Polluted Urban Area of China: Implications for Light Absorption Enhancement

Qiyuan Wang,[1] R.-J. Huang,[2,3] Junji Cao,[1,4] Yongming Han,[1] Gehui Wang,[1] Guohui Li,[1] Yichen Wang,[1] Wenting Dai,[1] Renjian Zhang,[5] and Yaqing Zhou[1]

[1]*Key Laboratory of Aerosol Science & Technology, SKLLQG, Institute of Earth Environment, Chinese Academy of Sciences, Xi'an, China*
[2]*Laboratory of Atmospheric Chemistry, Paul Scherrer Institute, Villigen PSI, Switzerland*
[3]*Centre for Climate and Air Pollution Studies, Ryan Institute, National University of Ireland Galway, Galway, Ireland*
[4]*Institute of Global Environmental Change, Xi'an Jiaotong University, Xi'an, China*
[5]*Key Laboratory of Regional Climate-Environment Research for Temperate East Asia, Institute of Atmospheric Physics, Chinese Academy of Sciences, Beijing, China*

Black carbon (BC) is important for climate forcing, and its effects on the Earth's radiative balance remain a major uncertainty in climate models. In this study, we investigated the mixing state of refractory black carbon (rBC) and aerosol optical properties in a polluted atmosphere at Xi'an, western China. The average rBC mass concentration was 9.9 μg m^{-3} during polluted periods, 7.6 times higher than that in clean periods. About 48.6% of the rBC was internally-mixed or coated with nonrefractory materials during polluted periods; this was 27% higher than in clean periods. Correlation analysis between the number fraction of thickly-coated rBC particles (f_{BC}) and the major particulate species indicate that organics may be the primary contributor to rBC coatings during polluted periods. The average mass absorption cross section of rBC (MAC_{BC}) particles at $\lambda = 870$ nm was 7.6 $\pm$ 0.02 m^2 g^{-1} for the entire campaign. The MAC_{BC} showed a positive correlation with f_{BC}, and the enhancement of MAC_{BC} due to internal mixing was 1.8 times. These observations suggest that an enhancement of BC absorption by a factor of $\sim$2 could be appropriate for climate models associated with high $PM_{2.5}$ levels.

1. INTRODUCTION

Black carbon (BC), the most efficient light-absorbing aerosol component in the atmosphere, is receiving increased interest due to its key role in radiative forcing (Jacobson 2001; Ramanathan and Carmichael 2008). Indeed, BC has been considered as the second largest contributor to anthropogenic radiative forcing after carbon dioxide (Jacobson 2001). The effects of BC on climate depend on not only its concentration but also the physical and chemical properties of the particles including their size, shape, and mixing state. For the latter, BC particles can acquire various substances as coatings, which enhances the particles' absorption of solar radiation compared with their uncoated counterparts (Bond et al. 2006; Moffet and Prather 2009). In this context, Jacobson (2000) estimated that the direct positive radiative forcing for internally-mixed BC particles is 0.78 W m^{-2}, which was about three times that for the externally-mixed BC particles (0.27 W m^{-2}). Moreover, coated BC particles can more readily act as cloud condensation nuclei (CCN), leading to more efficient removal by wet deposition (Jacobson 2010).

Eastern-southern Asia is one of the world's largest emitters of anthropogenic BC, in particular China accounts for $\sim$60% of the Asian emissions (Zhang et al. 2009). Due to the short atmospheric lifetimes of BC particles, regional effects of BC on light absorption are of particular concern. Modeling studies suggested that the direct BC-induced radiative forcing in the atmosphere over China was of the order of $\sim$5 W m^{-2} (Chung and Seinfeld 2005). Despite numerous studies of BC in China, most studies have made use of filter-based instruments to measure bulk aerosol absorption rather than direct measurements of BC mass concentrations (Cheng et al. 2006; Cao et al. 2009). Filter-based absorption techniques are subject to a number of systematic errors (Arnott et al. 2005), and is incapable of providing information on the BC mixing state. Recent assessments of aerosol radiative effects have highlighted the

Received 22 July 2013; accepted 10 April 2014.
Address correspondence to Junji Cao, Key Laboratory of Aerosol Science & Technology, SKLLQG, Institute of Earth Environment, Chinese Academy of Sciences, Xi'an 710075, China. E-mail: cao@loess.llqg.ac.cn
Color versions of one or more figures in this article can be found online at www.tandfonline.com/uast.

need for better measurements of BC mass concentrations and optical properties which are crucial for reducing the uncertainties in climate models.

Heavy pollution episodes, also known as haze-fog events, covered an area of >1 million km^2 over China in January 2013, leading to worldwide attention to the seriousness of particulate pollution in China. A set of measurements was performed in Xi'an, China to investigate individual refractory black carbon (rBC) particles and aerosol optical properties during the severe air pollution events. These analyses were made with the use of a single-particle soot photometer (SP2) and a photoacoustic extinctiometer (PAX), respectively. Additionally, an aerosol chemical speciation monitor (ACSM) was used to provide more detailed information on the substances mixed with the rBC. The main objectives of the study were (1) to quantify rBC mass concentrations and determine the rBC mixing state, (2) to derive rBC mass absorption cross sections, and (3) to characterize the relationship between the rBC mixing state and optical properties.

2. EXPERIMENTAL

2.1. Research Site

Xi'an, located on the Guanzhong Plain at the southern edge of the Loess Plateau (33°29′ to 34°44′N, 107°40′ to 109°49′, and ~400 m above sea level), is the largest city in northwestern China and has a population of >8 million. For many years, the city has suffered from high loadings of aerosol particles, which are primarily emitted from coal combustion, motor vehicle emissions, and biomass burning in the suburbs (Shen et al. 2009). Heavy pollution episodes frequently occurred at Xi'an in the winter of 2012–2013, and they were among the worst in the country (http://datacenter.mep.gov.cn). For our studies of rBC, measurements were made from the rooftop (~10 m above ground level) of the Institute of Earth Environment, Chinese Academy of Sciences (IEECAS; Figure S1 in the online supplementary information) from 23 December 2012 to 18 January 2013. Figure S1 shows the schematic of measurements system. This site is ~15 km southwest of downtown Xi'an; it is surrounded by a residential/commercial area and is most representative of urban-scale conditions according to the criteria of Chow et al. (2002).

2.2. rBC Mass and Mixing State Measurements

The SP2 used for the rBC measurements is a commercially available instrument (Droplet Measurement Technologies, Boulder, CO, USA), and its operation has been described in detail previously (Schwarz et al. 2006; Gao et al. 2007). Briefly, the SP2 uses intracavity Nd:YAG laser light at 1064 nm to quantify the rBC mass in individual rBC-particles. When an rBC-containing particle passes through the laser beam, the rBC component is heated to its vaporization temperature, and this causes the emission of incandescent light. The rBC mass is linearly related to the incandescence signal, irrespective of the particle morphology or mixing state (Slowik et al. 2007). In our study, the incandescence signal was calibrated using a standard fullerene soot sample (Lot F12S011, AlphaAesar, Inc., Ward Hill, MA, USA), which was size separated by incorporating a differential mobility analyzer (EPS-20 Electrical Particle Size, HCT, Korea) upstream of the SP2. The calibration curve was obtained from the peak intensity of the incandescence signal for the fullerene soot particles with diameters ranging from 80 to 450 nm.

The light-scattering signals of the SP2 were calibrated by introducing different sizes of monodisperse polystyrene latex spheres (PSL) into the instrument. The laser intensity was monitored by analyzing PSL particles of a specific diameter (269 nm) throughout the experiment; this was done to ensure the stability of the SP2 for the proper detection of rBC (Schwarz et al. 2010). Here, the rBC cores in a mass range of ~0.4–1050 fg, equivalent to ~70–1000 nm volume-equivalent diameters were quantified assuming the particles were solid spheres with a density of 2.0 g cm^{-3}. Figure S2 shows that approximately 90% of total rBC mass was detected by the SP2 based on a lognormal fit of the mass-particle size distribution. The remaining mass was associated with particles below the size-detection limit of the SP2. Thus, to estimate the total rBC mass, we increased the SP2 mass values by a scaling factor of 1.1 throughout the dataset. The uncertainty in the rBC mass determinations was ~25% due to uncertainties in the rBC mass calibration, flow measurements, and estimation of rBC mass outside of SP2 detection range.

The SP2 also provides information on the rBC mixing state. The lagtime method (the time of the peak of the incandescence signal minus the time of the peak of the scattering signal) is a commonly used approach for distinguishing between "thickly-" and "thinly-coated" single rBC particles (McMeeking et al. 2011; Perring et al. 2011; Wang et al. 2014). This is commonly expressed as the number fraction of thickly-coated rBC particles (f_{BC}), that is, the ratio of the number of thickly-coated rBC particles to the sum of thickly-coated and thinly-coated particles. The principle behind this method is that the lagtime increases when larger amounts of non-refractory material are present. In this study, the time criterion for distinguishing uncoated or thinly-coated rBC from thickly-coated rBC is 2 μs, based on the observed minimum in the bimodal frequency distribution of delay times (Moteki et al. 2007).

2.3. Particle Light Absorption Measurements

The PAX (Droplet Measurement Technologies, Boulder, CO, USA) directly measures in-situ aerosol light absorption (σ_{abs}) every minute using intracavity photoacoustic technology. A laser beam in the acoustic chamber of the instrument heats absorbing aerosol particles, and this heating produces pressure waves that are detected with a microphone. The

sensors in the instrument, including a nephelometer for measuring the light scattering coefficient, make use of phase-sensitive detection. In this study, the light absorption at $\lambda = 870$ nm was measured with the PAX. The instrument is also capable of independently measuring the extinction coefficient using the laser power: to this end, freshly-generated propane soot was used to give an absorption reading of 5000–10,000 Mm^{-1} for the σ_{abs} calibration. A correction factor was then established from the relationship between the extinction-minus-scattering coefficient and σ_{abs}.

2.4. Aerosol Chemical Measurements

An Aerosol Chemical Speciation Monitor (ACSM, Aerodyne Research Inc., Billerica, MA, USA) was used to measure the mass concentrations and composition of non-refractory submicron aerosols (NR-PM_1) including organics, SO_4^{2-}, NO_3^-, NH_4^+, and Cl^-. The ACSM focuses individual particles (~40–1000 nm aerodynamic diameter) into a beam, and non-refractory components are vaporized, ionized, and finally analyzed with a quadrupole mass spectrometer. The chemically-speciated aerosol mass loadings are then extracted from the mass spectra. A collection efficiency of 0.5 was used to account for the incomplete detection of aerosol particles, which is mainly due to particle bounce at the vaporizer (Middlebrook et al. 2012). More detailed descriptions of the operating principles of the ACSM can be found in Ng et al. (2011).

2.5. Meteorological Conditions and Classification of Events

The standards issued by the China Meteorological Administration (2010) define haze (also referred to as a polluted period here) as a condition in which the visibility and relative humidity (RH) are less than 10 km and 80%, respectively. These two meteorological variables along with wind speed and $PM_{2.5}$ loadings were monitored simultaneously as part of our study. Information on the instruments used for these measurements is included in Table 1. A plot of the variations of $PM_{2.5}$ mass concentrations, visibility, and RH (Figure S3) shows that haze events occurred during nearly 90% of the sampling period. As shown in Table 2, the average $PM_{2.5}$ concentration during the clean periods was 32 $\mu g\ m^{-3}$, and the average loadings reached as high as 214 $\mu g\ m^{-3}$ during polluted periods of the entire campaign.

The transitions between clean and polluted periods were strongly linked to changes in synoptic meteorology. During

Table 1
A summary of the instrumental analysis during the measurement campaign

Instruments	Contents[a]	Resolution	Particle type	Instrument principle
Single Particle Soot Photometer	Refractory black carbon (rBC)	15 min	$PM_{2.5}$ cyclone	Intracavity Nd:YAG laser light at 1064 nm to quantify the rBC mass in individual rBC-particles.
Photoacoustic Extinctiometer	Absorption/scattering coefficient	15 min	$PM_{2.5}$ cyclone	A laser beam in the acoustic chamber of the instrument heats absorbing aerosol particles, and this heating produces pressure waves that are detected with a microphone.
Aerosol Chemical Speciation Monitor	Organics, SO_4^{2-}, NO_3^-, NH_4^+, and Cl^-	1 h	$PM_{2.5}$ cyclone	Individual particles (~40–1000 nm) into a beam, and non-refractory components are vaporized, ionized, and finally analyzed with a quadrupole mass spectrometer.
Environmental Beta Attenuation Monitor	$PM_{2.5}$	1 h	$PM_{2.5}$ impactor	Attenuation of beta ray energy as aerosol mass accumulates.
Automatic Weather Station	Visibility, humidity, wind, temperature	1 min		Visibility sensor (Model PWD22), RH/temperature probe (Model QMH101), and wind sensor (Model QMW101-M2).

[a]The concentrations of $PM_{2.5}$, rBC, organics, SO_4^{2-}, NO_3^-, NH_4^+, and Cl^- as well as light absorption, were corrected to standard temperature and pressure (STP: 273.15 K, 1013.25 hPa).

Table 2
Summary of rBC concentrations and number fraction of thickly coated rBC particles (f_{BC}) as well as related chemical concentrations of particulate matter

	Clean periods		Polluted periods		All samples	
Parameter	Mean	SD	Mean	SD	Mean	SD
rBC (μg m^{-3})	1.3	0.7	9.9	7.3	8.8	7.3
f_{BC} (%)	38.3	5.7	48.6	6.9	47.4	7.6
Organics (μg m^{-3})	13.8	6.8	82.1	49.7	73.8	46.8
SO_4^{2-} (μg m^{-3})	2.9	1.4	31.3	23.2	18.3	15.3
NO_3^- (μg m^{-3})	2.9	1.8	17.0	8.6	13.6	7.6
NH_4^+ (μg m^{-3})	3.7	1.5	23.5	13.0	16.7	10.0
Cl^- (μg m^{-3})	1.4	0.9	8.7	5.4	7.6	5.4
$PM_{2.5}$ (μg m^{-3})	31.9	17.3	213.6	115.8	191.2	123.9

Clean periods: visibility greater than 10 km.
Polluted periods: visibility less than 10 km.
SD: standard deviation.

polluted periods, the surface winds were weak, and the atmospheric vertical motions were predominantly downdrafts (Figure S4). The horizontal and vertical dispersal of contaminants were both restricted under such conditions, leading to the accumulation of pollutants in the surface layer. In contrast, cold-air incursions during clean periods led to low temperatures and slightly stronger winds; those conditions were more favorable with respect to pollutant dilution and transport.

3. RESULTS AND DISCUSSION

3.1. rBC Mass Loadings

Time-resolved (15 min) variations in rBC mass loadings are shown in Figure S3, and a statistical summary of the data is presented in Table 2. The daily rBC concentrations during the sampling period were highly variable, with a range from 0.3 to 44.5 μg m^{-3} and an average (arithmetic mean) value ($\pm$ standard deviation) of 8.8 $\pm$ 7.3 μg m^{-3}. The average rBC concentration during polluted periods (9.9 μg m^{-3}) was 7.6 times higher than that during clean periods (1.3 μg m^{-3}). Compared with SP2-based measurements from other urban areas in China, the average rBC concentrations in Xi'an is 1.1–4.0 times higher than Jiaxing (7.1 μg m^{-3}, Huang et al. 2013), Shenzhen (4.1 μg m^{-3}, Huang et al. 2012a), and Shanghai (2.0 μg m^{-3}, Huang et al. 2012b). Additionally, it is orders-of-magnitude higher than SP2-based measurements reported for the lower troposphere in Europe (0.05–0.3 μg m^{-3}, McMeeking et al. 2010), Texas (0.34 μg m^{-3}, Schwarz et al. 2009), and several remote areas, including Qinghai Lake (0.36 μg m^{-3}, Wang et al. 2014), Fukue Island (0.32 μg m^{-3}, Shiraiwa et al. 2008) and the Jungfraujoch (0.004–0.033 μg m^{-3}, Liu et al. 2010). The high rBC loadings at Xi'an may be attributed to the large quantities of coal burning for wintertime heating combined with stable meteorological conditions in winter.

A plot of the hourly variations in rBC loadings (Figure 1) shows that the median and mean rBC values exhibited the same diurnal pattern, that is, "two peaks and two valleys." This diurnal variability can be explained by the daily cycles in boundary-layer mixing as well as the activity patterns of daily life. The maximum rBC values in the early morning (07:00–09:00 LST) can be attributed to rush-hour traffic, and this is generally consistent with atmospheric variations observed in other urban areas (Huang et al. 2012a). The mean rBC levels were considerably higher than the medians during the rush hour, suggesting that the elevated rBC loadings were largely event driven. Later in the day, the depth of the boundary layer increased due to solar heating, leading to the mixing of clean air from above with polluted air below. As a result, the mixing-induced dilution led to a minimum in rBC loadings during the afternoon (14:00–16:00 LST). The relatively shallow boundary layer at night trapped locally-produced pollutants near the surface, and this led to another peak in rBC concentrations in the late evening (22:00–23:00 LST).

Figure S5 shows that the rBC concentrations varied with wind direction and wind speed. When the winds were from the northeast and northwest with speeds >2.0 m s^{-1}, the rBC concentrations were low. This result indicates that at times regional transport from northeast and northwest brought relatively clean air to Xi'an. In contrast, when the winds were from northwest and weak (<1 m s^{-1}), the rBC concentrations reached their highest values. Therefore, the strongest primary rBC emissions were most likely local and the sources located to the northwest of the observation site. Indeed, there are several polluting enterprises in that upwind sector (Figure S1). When the winds were from the northeast and wind speeds ranged from 1 to 2 m s^{-1}, the rBC concentrations showed intermediate values.

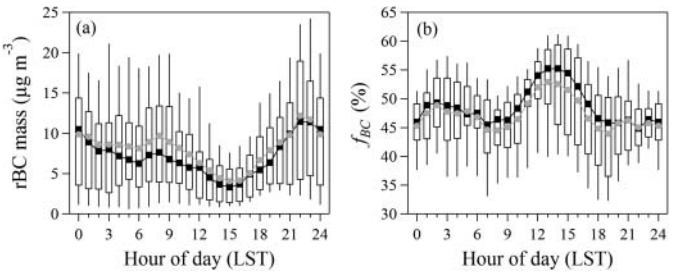

FIG. 1. (a) Hourly variations of rBC mass concentration and (b) number fraction of thickly coated rBC particles (f_{BC}). In each panel, the lower and upper edges of the boxes denote the 25% and 75% percentiles, respectively. The black and grey lines indicate the median and mean values, with vertical bars showing the 10th and 90th percentiles. LST stands for local standard time.

3.2. rBC Mixing State

Knowledge of the BC mixing state is critical for developing realistic simulations of the direct radiative effects of the aerosol as well as their forcing effects on climate (Mallet et al. 2004). As shown in Figure S3 and Table 2, f_{BC}, expressed as a percentage, ranged from 18.3–68.8%, with an average value of 47.4% for the entire campaign period. The average f_{BC} during clean periods was 38.3%, indicating that fresh, uncoated or thinly-coated rBC particles constituted the bulk of the rBC aerosol under those conditions. However, f_{BC} increased to 48.6% during polluted periods, about 27% higher compared with clean periods.

Interestingly, f_{BC} exhibited a diurnal pattern that was opposite to that seen in the rBC concentrations themselves (Figure 1). An increase in thickly-coated rBC was observed between 12:00–15:00 LST, likely due to the increase of secondary aerosol formed from enhanced photochemical oxidation promoted by higher solar irradiance. There were two valleys in f_{BC}, one occurred in the early morning rush hours and the other during the evening rush hours. This indicates the large vehicular emissions of fresh and externally-mixed rBC particles that are not yet subject to substantial aging.

The dependence of f_{BC} on wind speed and direction is shown in Figure S5. High f_{BC} values are generally associated with the low wind-speed region without an apparent dependence on wind direction. This implies that locally-emitted rBC particles age rapidly under stagnant weather conditions, leading to the formation of coatings from other chemical species. Figure S5 also shows a lobe of elevated f_{BC} values when the wind is from the northeast with a speed >2 m s^{-1}. This suggests that aged rBC particles are brought to the site by regional transport at times overwhelming the fresh, locally-emitted rBC particles, especially when the rBC loadings are low.

Previous studies have used a positive matrix factorization (PMF) model to evaluate the contributions of different aerosol chemical species to the coatings on rBC particles (Shiraiwa et al. 2008; Metcalf et al. 2012). The principles of PMF have been described in detail elsewhere (Paatero and Tapper 1994). The ratios of the mass concentrations of organics, SO_4^{2-}, NO_3^-, and NH_4^+ to the corresponding rBC loadings and the f_{BC} values are the data input to the PMF model. The values predicted by the PMF model, including the organics/rBC, SO_4^{2-}/rBC, NO_3^-/rBC, and NH_4^+/rBC ratios and f_{BC} agree well with the observed values: the correlation coefficients are 0.75, 0.99, 0.99, 0.97, and 0.91, respectively.

The PMF model was run multiple times, and the three-factor solution is the most physically interpretable profiles (Figure 2a). Factor 1 is characterized with high loading for NO_3^-/rBC indicating that NO_3^- may be the main contributor to this coating-related factor. Factor 2 is dominated by organics/rBC, and therefore organics are likely the major contributor to the coatings associated with this factor. Factor 3 is most heavily loaded with SO_4^{2-}/rBC, suggesting that SO_4^{2-} may be the main contributor to rBC coatings in this factor.

Figure 2b shows that Factors 1 and 2 contribute predominantly to f_{BC} over the course of the study, and therefore the nitrate and organics evidently are the two most important components of the coatings. These two factors combined account for 87.8% of the coatings on rBC aerosols, with Factors 1 (NO_3^-) and 2 (organics) amounting for 30.2% and 57.6% of the total coating mass, respectively. For the samples collected under clean conditions, Factor 1 increases to 41.0%, while for polluted samples, Factor 2 increases to 59.4%. The contribution of Factor 3 remains relatively stable throughout the study.

3.3. Particle Light Absorption and rBC

The mass absorption cross section of the BC aerosol (MAC_{BC}, expressed here in m^2 g^{-1}) is an important characteristic of the BC particles because it links their optical properties to their mass. Previous studies demonstrate that BC, brown carbon and mineral dust are the most important light absorption aerosols, and their light absorption properties are

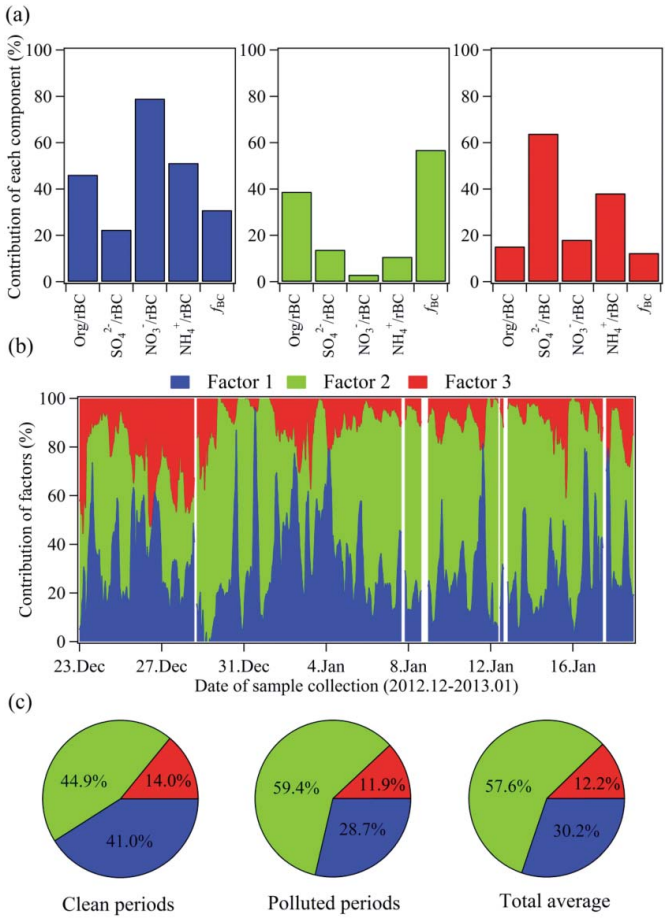

FIG. 2. (a) Contributions of organic/rBC, SO_4^{2-}/rBC, NO_3^-/rBC, NH_4^+/rBC, and f_{BC} in the three-factor PMF model; (b) time series of factor contributions to the f_{BC}; (c) contributions of each factor to f_{BC} during clean and polluted periods.

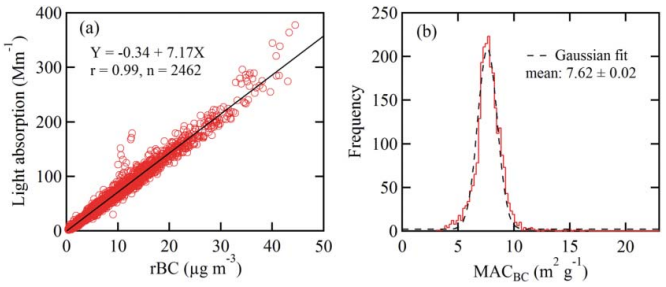

FIG. 3. (a) The linear relationship between light absorption and rBC concentration during the campaign. (b) Frequency distribution of rBC mass absorption cross section (MAC_{BC}).

distinctive functions of the wavelengths of light (Yang et al. 2009; Lack and Cappa 2010). Therefore, the relationship among σ_{abs}, MAC_{BC} and BC concentration can be described by the following equation:

$$\sigma_{abs} = MAC_{BC} \times [BC] + \sigma_{abs\_others} \quad [1]$$

where [BC] is the mass concentration of BC particles, and σ_{abs_others} represents the light absorption contributed by non-BC materials (e.g., brown carbon and soil dust). Plot of the linear regression of σ_{abs} ($\lambda = 870$ nm) as a function of the rBC mass is shown in Figure 3a. Strong correlation ($r = 0.99$) between these two variables is found for the entire campaign. The intercept of the fitting line is close to zero, indicating that σ_{abs_others} from other materials is very small and BC is the main contributor to light absorption at $\lambda = 870$ nm. Therefore, the MAC_{BC} can be estimated from the ratio of σ_{abs} at $\lambda = 870$ nm and rBC mass. As shown in Figure 3b, the MAC_{BC} values exhibits Gaussian distribution with a mean value of 7.6 ± 0.02 m^2 g^{-1}.

Table 3 summarizes the MAC_{BC} values determined from previous studies, including information on the measurement methods used. The MAC_{BC} values vary widely, even for studies using the same wavelength of light. The apparent site-to-site variability in MAC_{BC} may be explained by differences in emission sources and combustion conditions as well as BC particle size and coatings (Bond and Bergstrom 2006; Gao et al. 2008; Schwarz et al. 2008). Further, different measurement methods for absorption and BC mass may also lead to the discrepancies among studies. As shown in Table 3, most of the MAC_{BC} measurements were made using filter-based absorption instruments. These approaches measure σ_{abs} based on the attenuation of light passing through an aerosol-loaded filter, and therefore are subject to a number of uncertainties (Arnott et al. 2005). The PAX used in our study, however, is a filter-free instrument, which is insensitive to light scattering.

3.4. Light Absorption Enhancement as a Function of rBC Mixing State

The absorption of solar and reflection of radiation by aerosols are closely related (not directly proportional) to positive climate forcing (Bond et al. 2006). There are evidences that the absorption of BC can be significantly enhanced by the internal mixing of BC with other substances. For example, Zhang et al. (2008) show that the internal mixing of BC particles with sulfuric acid result in the enhancement of light

Table 3
Comparison of mass absorption cross sections of BC (MAC_{BC}) from different studies

Location	Type of sample	Sampling period	Measurement technique[a]		λ (nm)[b]	MAC (m^2 g^{-1})	Reference
			σ_{abs}	BC			
Xi'an, China	Urban	December 2012–January 2013	PAX	SP2	870	7.6	This study
Shenzhen, China	Urban	August–September 2011	PASS	SP2	532	6.5	Lan et al. 2013
Fresno Supersite, USA	Urban	August–September 2005	PASS	EC/OC analyzer	532	8.1	Chow et al. 2009
Pasadena, CA, USA	Urban	May–June 2010	AE	EC/OC analyzer	532	5.7	Thompson et al. 2012
The Jungfraujoch, Switzerland	Remote	February–March 2007	MAAP	SP2	630	10.2	Liu et al. 2010
United Kingdom	Plumes	April 2008	PSAP	SP2	550	15.4	McMeeking et al. 2011
Mexico City	Plumes	March 2006	PSAP	SP2	660	10.6	Subramanian et al. 2010

[a]PAX: Photoacoustic extinctiometer; PASS: photoacoustic soot spectrometer; PSAP: particle soot absorption photometer; MAAP: multi-angle absorption photometer; AE: aerosol extinction; SP2: single particle soot photometer.
[b]λ stands for wavelength of light.

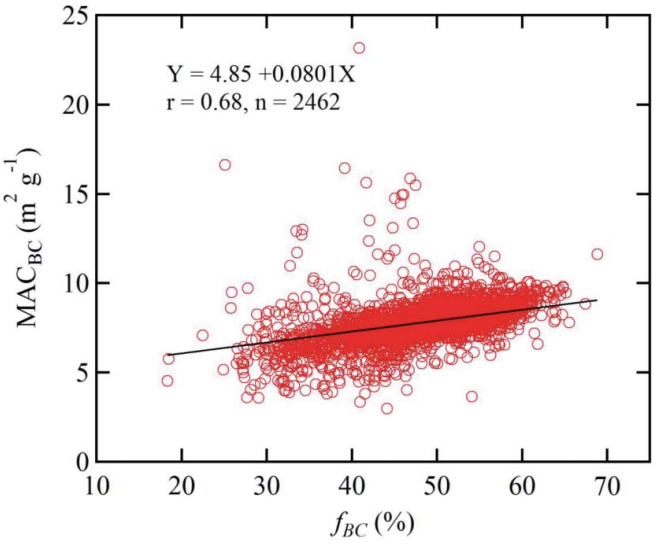

FIG. 4. The rBC mass absorption cross section (MAC_{BC}) as function of number fraction of thickly coated rBC (f_{BC}).

absorption by nearly two-fold at 80% RH compared with fresh BC particles. In a laboratory study, Shiraiwa et al. (2010) found a twofold absorption enhancement for BC particles with thick coatings of organic compounds. Chamber studies also show an absorption enhancement of 1.8–2.1 times when diesel BC particles are coated with secondary organic compounds (Schnaiter et al. 2005).

To investigate the potential influence of the rBC mixing state on light absorption, the MAC_{BC} values are plotted against f_{BC} (Figure 4). In order to reduce the impact of outlier data, a robust regression method is used to get the experimental growth curve (Miconnet et al. 2005). As shown in Figure 4, the MAC_{BC} is significantly correlated ($r = 0.68$, $p < .001$) with f_{BC}, indicating an enhancement of light absorption for coated rBC particles. If the results from the linear regression shown in Figure 4 are extrapolated to a condition where the rBC is completely externally mixed (that is, f_{BC} or $x = 0$), the MAC_{BC} would be 4.9 $m^2\ g^{-1}$. The MAC_{BC} for uncoated particles estimated in this way is consistent with the value of 4.7 $m^2\ g^{-1}$ (interpolated to 870 nm from 550 nm assuming an Absorption Ångström Exponent of 1.0) suggested by Bond and Bergstrom (2006) for uncoated BC particles. Furthermore, the MAC_{BC} calculated for the opposite case, that is, all rBC being internally mixed (f_{BC} or $x = 100\%$), would be 12.9 $m^2\ g^{-1}$. This would represent the maximum potential effect on absorption, and it would represent an amplification of the MAC_{BC} with a factor of 2.7 compared with the fully externally-mixed and uncoated BC particles. The observed average rBC mixing state during the campaign is $f_{BC} = 47.4\%$, therefore the enhancement of MAC_{BC} calculated from the regression model would be a factor of 1.8.

Our observations therefore indicate that climate models, which assume around twofold enhancement of BC absorption from internal-mixing of BC, may be appropriate for high $PM_{2.5}$ loadings. Nevertheless, Cappa et al. (2012) report that the rBC absorption enhancements at two regions of California are rather small (6%) based on direct *in situ* measurements. Lan et al. (2013) also observed a small enhancement (7%) of absorption in the urban atmosphere of Shenzhen, China. The authors suggested that rBC absorption enhancement due to internal mixing in the atmosphere is relatively low and that many climate models may overestimate the warming effect from BC. The reasons for the large discrepancies between studies could be manifold: (i) the levels of particulate pollution and the main species of pollutants could be different in space and time; (ii) changes in particle size may offset the expected enhancement in absorption due to internally-mixed BC under low chemical loadings.

4. CONCLUSIONS

This study investigates the rBC mass and mixing state as well as the rBC mass absorption cross section in the heavily polluted atmosphere of Xi'an, the largest city in northwestern China. The studies, conducted from 23 December 2012 to 18 January 2013, show a rBC mass concentration of 9.9 $\mu g\ m^{-3}$ during polluted periods, ~7.6 times higher than that in clean periods. High rBC concentrations are observed when the winds are from northwest at low speed (<1 $m\ s^{-1}$). Results obtained with a single-particle soot photometer show that 38.3% of the rBC particles are thickly-coated during clean conditions, but this fraction increases to 48.6% during polluted periods. An increase in thickly-coated rBC particles is evident in the afternoon mainly due to the enhanced photochemical oxidation to form secondary aerosol under stronger solar irradiation.

The PMF model simulations show that organics and nitrate are most likely the main contributors to the rBC coatings, with the contribution from organics increasing further during polluted periods. The average MAC_{BC} derived from the PAX and SP2 measurements is 7.6 ± 0.02 $m^2\ g^{-1}$ during the entire campaign period. The MAC_B is positively correlated ($r = 0.68$) with f_{BC}, and the empirically-determined relationship shows that the MAC_{BC} may increase with a factor of 1.8 due to the internal mixing of rBC with other species. Therefore, an enhancement factor of ~2 for BC absorption due to internal mixing may be appropriate for modeling studies of polluted atmospheres.

The mixing state and physicochemical properties of BC are important because of the regional effects on light absorption discussed above. In addition, high BC concentrations also have important implications for human health (Pope and Dockery 2006; Cao et al. 2012). The internal mixing of rBC with other substances in the atmosphere may have important consequences in terms of biological effects, including those on human health, but these are largely unclear. Therefore, the impacts of BC particle pollution on biological systems are

another field in which the results of our study of BC and its mixing with other substances may be meaningful.

ACKNOWLEDGMENTS

The authors would like to thank Dr. Rushan Gao from NOAA and two anonymous reviewers for their helpful comments on the manuscript.

FUNDING

This study was supported by the National Natural Science Foundation of China (41230641, 40925009) and projects from the "Strategic Priority Research Program" of the Chinese Academy of Science (Grant No. XDA05100401) and the Shaanxi Government (2012KTZB03-01-01, 2011KTCQ03-04).

SUPPLEMENTAL MATERIAL

Supplemental data for this article can be accessed on the publisher's website.

REFERENCES

Arnott, W. P., Hamasha, K., Moosmüller, H., Sheridan, P. J., and Ogren, J. A. (2005). Towards Aerosol Light-Absorption Measurements with a 7-Wavelength Aethalometer: Evaluation with a Photoacoustic Instrument and 3-Wavelength Nephelometer. *Aerosol Sci. Technol.*, 39:17–29.

Bond, T. C., and Bergstrom, R. W. (2006). Light Absorption by Carbonaceous Particles: An Investigative Review. *Aerosol Sci. Technol.*, 40:27–67.

Bond, T. C., Habib, G., and Bergstrom, R. W. (2006). Limitations in the Enhancement of Visible Light Absorption Due to Mixing State. *J. Geophys. Res.*, 111:D20211, doi:10.1029/2006JD007315.

Cao, J. J, Xu, H. M, Xu, Q., Chen, B. H., and Kan, H. D. (2012). Fine Particulate Matter Constituents and Cardiopulmonary Mortality in a Heavily Polluted Chinese City. *Environ. Health Persp.*, 120:373 3–378. doi:10.1289/ehp.1103671.

Cao, J. J., Zhu, C. S., Chow, J. C., Watson, J. G., Han, Y. M., Wang, G., et al. (2009). Black Carbon Relationships with Emissions and Meteorology in Xi'an, China. *Atmos. Res.*, 94:194–202.

Cappa, C. D., Onasch, T. B., Massoli, P., Worsnop, D. R., Bates, T. S., Cross, E. S., et al. (2012). Radiative Absorption Enhancements Due to the Mixing State of Atmospheric Black Carbon. *Science*, 337:1078–1081.

Cheng, Y., Lee, S. C., Ho, K. F., Wang, Y. Q., Cao, J. J., Chow, J. C., et al. (2006). Black Carbon Measurement in a Coastal Area of South China. *J. Geophys. Res.*, 111:D12310, doi: 10.1029/2005JD006663.

China Meteorological Administration (2010). Observation and Forecasting Levels of Haze. QX/T 113-2010 (in Chinese).

Chow, J. C., Engelbrecht, J. P., Watson, J. G., Wilson, W. E., Frank, N. H., and Zhu, T. (2002). Designing Monitoring Networks to Represent Outdoor Human Exposure. *Chemosphere*, 49:961–978.

Chow, J. C., Watson, J. G., Doraiswamy, P., Chen, L.-W. A., Sodeman, D. A., Lowenthal, D. H., et al. (2009). Aerosol Light Absorption, Black Carbon, and Elemental Carbon at the Fresno Supersite, California. *Atmos. Res.*, 93:874–887.

Chung, S. H., and Seinfeld, J. H. (2005). Climate Response of Direct Radiative Forcing of Anthropogenic Black Carbon. *J. Geophys. Res.*, 110:D11102, doi: 10.1029/2004JD005441.

Gao, R. S., Hall, S. R., Swartz, W. H., Schwarz, J. P., Spackman, J. R., Watts, L. A., et al. (2008). Calculations of Solar Shortwave Heating Rates Due to Black Carbon and Ozone Absorption using in Situ Measurements. *J. Geophys. Res.*, 113:D14203, doi:10.1029/2007JD009358.

Gao, R. S, Schwarz, J. P., Kelly, K. K., Fahey, D. W., Watts, L. A., Thompson, T. L., et al. (2007). A Novel Method for Estimating Light-Scattering Properties of Soot Aerosols using a Modified Single-Particle Soot Photometer. *Aerosol. Sci. Technol.*, 41:125–135.

Huang, X. F., He, L. Y., Xue, L., Sun, T. L., Zeng, L. W., Gong, Z. H., et al. (2012b). Highly Time-Resolved Chemical Characterization of Atmospheric Fine Particles During 2010 Shanghai World Expo. *Atmos. Chem. Phys.*, 12:4897–4907.

Huang, X. F., Sun, T. L., Zeng, L. W., Yu, G. H., and Luan, S. J. (2012a). Black Carbon Aerosol Characterization in a Coastal City in South China using a Single Particle Soot Photometer. *Atmos. Environ.*, 51:21–28.

Huang, X. F., Xue, L., Tian, X. D., Shao, W. W., Sun, T. L., Gong, Z. H., et al. (2013). Highly Time-Resolved Carbonaceous Aerosol Characterization in Yangtze River Delta of China: Composition, Mixing State and Secondary Formation. *Atmos. Environ.*, 64:200–207.

Lack, D. A., and Cappa, D. (2010). Impact of Brown and Clear Carbon on Light Absorption Enhancement, Single Scatter Albedo and Absorption Wavelength Dependence of Black Carbon. *Atmos. Chem. Phys.*, 10: 4207–4220.

Jacobson, M. Z. (2000). Physically-Based Treatment of Elemental Carbon Optics: Implications for Global Direct Forcing of Aerosols. *Geophys. Res. Lett.*, 27:217–220.

Jacobson, M. Z. (2001). Strong Radiative Heating Due to the Mixing State of Black Carbon in Atmospheric Aerosols. *Nature*, 409:695–697.

Jacobson, M. Z. (2010). Short-Term Effects of Controlling Fossil Fuel Soot, Biofuel Soot and Gases, and Methane on Climate, Arctic Ice, and Air Pollution Health. *J. Geophys. Res.*, 115:D14209, doi:10.1029/2009JD013795.

Lan, Z. J., Huang, X. F., Yu, K. Y., Sun, T. L., Zeng, L. W., and Hu, M. (2013). Light Absorption of Black Carbon Aerosol and Its Enhancement by Mixing State in an Urban Atmosphere in South China. *Atmos. Environ.*, 69:118–123.

Liu, D., Flynn, M., Gysel, M., Targino, A., Crawford, I., Bower, K., Choularton, T., Jurányi, Z., Steinbacher, M., Hüglin, C., et al. (2010). Single Particle Characterization of Black Carbon Aerosols at a Tropospheric Alpine Site in Switzerland. *Atmos. Chem. Phys.*, 10:7389–7407.

Mallet, M., Roger, J., Despiau, S., Putaud, J., and Dubovik, O. (2004). A Study of the Mixing State of Black Carbon in Urban Zone. *J. Geophys. Res.*, 109:D04202, doi: 10.1029/2003JD003940.

McMeeking, G., Hamburger, T., Liu, D., Flynn, M., Morgan, W., Northway, M., et al. (2010). Black Carbon Measurements in the Boundary Layer Over Western and Northern Europe. *Atmos. Chem. Phys.*, 10:9393–9414.

McMeeking, G., Morgan, W., Flynn, M., Highwood, E., Turnbull, K., Haywood, J., et al. (2011). Black Carbon Aerosol Mixing State, Organic Aerosols and Aerosol Optical Properties Over the United Kingdom. *Atmos. Chem. Phys.*, 11:9037–9052.

Metcalf, A. R., Craven, J. S., Ensberg, J. J., Brioude, J., Angevine, W., Sorooshian, A., et al. (2012). Black Carbon Aerosol Over the Los Angeles Basin During CalNex. *J. Geophys. Res.*, 117:D00V13, doi:10.1029/2011JD017255.

Miconnet, N., Geeraerd, A. H., Impe, J. F. V., Rosso, L., and Cornu, M. (2005). Reflections on the use of Robust and Least-Squares Non-Linear Regression to Model Challenge Texts Conducted in/on Food Products. *Int. J. Food Microbiol.*, 104:161–177.

Middlebrook, A. M., Bahreini, R., Jimenez, J. L., and Canagaratna, M. R. (2012). Evaluation of Composition-Dependent Collection Efficiencies for the Aerodyne Aerosol Mass Spectrometer using Field Data. *Aerosol Sci. Technol.*, 46:258–271.

Moffet, R. C., and Prather, K. A. (2009). In-Situ Measurements of the Mixing State and Optical Properties of Soot with Implications for Radiative Forcing Estimates. *P. Natl. Acad. Sci. USA*, 106:11872–11877.

Moteki, N., Kondo, Y., Miyazaki, Y., Takegawa, N., Komazaki, Y., Kurata, G., et al. (2007). Evolution of Mixing State of Black Carbon Particles: Aircraft Measurements Over the Western Pacific in March 2004. *Geophys. Res. Lett.*, 34:L11803, doi: 10.1029/2006GL028943.

Ng, N., Herndon, S., Trimborn, A., Canagaratna, M., Croteau, P., Onasch, T., et al. (2011). An Aerosol Chemical Speciation Monitor (ACSM) for Routine Monitoring of the Composition and Mass Concentrations of Ambient Aerosol. *Aerosol Sci. Technol.*, 45:780–794.

Paatero, P., and Tapper, U. (1994). Positive Matrix Factorization: A Non-Negative Factor Model with Optimal Utilization of Error Estimates of Data Values. *Environmetrics,* 5:111–126.

Perring, A. E., Schwarz, J. P., Spackman, J. R., Bahreini, R., de Gouw, J. A., Gao, R. S., et al. (2011). Characteristics of Black Carbon Aerosol from a Surface Oil Burn During the Deepwater Horizon Oil Spill. *Geophys. Res. Lett.*, 38:L17809, doi: 10.1029/2011GL048356.

Pope, C. A. III, and Dockery, D. W. (2006). Critical Review: Health Effects of Fine Particulate Air Pollution: Lines That Connect. *J. Air Waste Manage.*, 56:709–742.

Ramanathan, V., and Carmichael, G. (2008). Global and Regional Climate Changes Due to Black Carbon. *Nature Geosci.*, 1:221–227.

Schnaiter, M., Linke, C., Möhler, O., Naumann, K. H., Saathoff, H., Wagner, R., Schurath, U., et al. (2005). Absorption Amplification of Black Carbon Internally Mixed with Secondary Organic Aerosol. *J. Geophys. Res.*, 110: D19204, doi: 10.1029/2005JD006046.

Schwarz, J. P., Gao, R. S., Fahey, D. W., Thomson, D. S., Watts, L. A., Wilson, J. C., et al. (2006). Single-Particle Measurements of Midlatitude Black Carbon and Light-Scattering Aerosols from the Boundary Layer to the Lower Stratosphere. *J. Geophys. Res.*, 111:D16207, dio: 10.1029/2006JD007076.

Schwarz, J. P., Spackman, J. R., Fahey, D. W., Gao, R. S., Lohmann, U., Stier, P., et al. (2008). Coatings and Their Enhancement of Black Carbon Light Absorption in the Tropical Atmosphere. *J. Geophys. Res.*, 113:D03203, doi: 10.1029/2007JD009042.

Schwarz, J. P., Spackman, J. R., Gao, R. S., Perring, A. E., Cross, E., Onasch, T. B., et al. (2010). The Detection Efficiency of the Single Particle Soot Photometer. *Aerosol Sci. Technol.*, 44:612–628.

Schwarz, J. P., Stark, H., Spackman, J. R., Ryerson, T. B., Peischl, J., Swartz, W. H., et al. (2009). Heating Rates and Surface Dimming Due to Black Carbon Aerosol Absorption Associated with a Major US City. *Geophys. Res. Lett.*, 36:L15807, doi: 10.1029/2009GL039213.

Shen, Z. X., Cao, J. J., Arimoto, R., Han, Z. W., Zhang, R. J., Han, Y. M., et al. (2009). Ionic Composition of TSP and $PM_{2.5}$ During Dust Storms and Air Pollution Episodes at Xi'an, China. *Atmos. Environ.*, 43:2911–2918.

Shiraiwa, M., Kondo, Y., Iwamoto, T., and Kita, K. (2010). Amplification of Light Absorption of Black Carbon by Organic Coating. *Aerosol Sci. Technol.*, 44:46–54.

Shiraiwa, M., Kondo, Y., Moteki, N., Takegawa, N., Sahu, L., Takami, A., et al. (2008). Radiative Impact of Mixing State of Black Carbon Aerosol in Asian Outflow. *J. Geophys. Res.*, 113:D24210, doi:10.1029/2008JD010546.

Slowik, J. G., Cross, E. S., Han, J. H., Davidovits, P., Onasch, T. B., Jayne, J. T., et al. (2007). An Inter-Comparison of Instruments Measuring Black Carbon Content of Soot Particles. *Aerosol Sci. Technol.*, 41:295–314.

Subramanian, R., Kok, G., Baumgardner, D., Clarke, A., Shinozuka, Y., Campos, T., et al. (2010). Black Carbon Over Mexico: The Effect of Atmospheric Transport on Mixing State, Mass Absorption Cross-Section, and BC/CO Ratios. *Atmos. Chem. Phys.*, 10:219–237 10.

Thompson, J. E., Hayes, P. L., Jimenez, J. L., Adachi, K., Zhang, X. L., Liu, J. M., et al. (2012). Aerosol Optical Properties at Pasadena, CA During CalNex 2010. *Atmos. Environ.*, 55:190–200.

Wang, Q. Y., Schwarz, J. P., Cao, J. J., Gao, R. S., Fahey, D. W., Hu, T. F., et al.(2014). Black Carbon Aerosol Characterization in a Remote Area of Qinghai-Tibetan Plateau, Western China. *Sci. Total Environ.*, 479–480:151–158.

Yang, M., Howell, S. G., Zhuang, J., and Huebert, B. J. (2009). Attribution of Aerosol Light Absorption to Black Carbon, Brown Carbon, and Dust in China – Interpretations of Atmospheric Measurements During EAST-AIRE. *Atmos. Chem. Phys.*, 9:2035–2050.

Zhang, Q., Streets, D. G., Carmichael, G. R., He, K. B., Huo, H., Kannari, A., et al. (2009). Asian Emissions in 2006 for the NASA INTEX-B Mission. *Atmos. Chem. Phys.*, 9:5131–5153.

Zhang, R., Khalizov, A. F., Pagels, J., Zhang, D., Xue, H., and McMurry, P. H. (2008). Variability in Morphology, Hygroscopicity, and Optical Properties of Soot Aerosols During Atmospheric Processing. *P. Natl. Acad. Sci. USA*, 105:10291–10296.